Chemical Engineering Journal 157 (2010) 67–72

Contents lists available at ScienceDirect

Chemical Engineering Journal

journal homepage: www.elsevier.com/locate/cej

Azeotropic distillation-assisted preparation of nanoscale gamma-alumina powder from waste oil shale ash

Baichao An, Guijuan Ji, Wenying Wang, Shucai Gan*, Jijing Xu, Guimei Gao, Guanghuan Li

College of Chemistry, Jilin University, 6 Ximinzhu street, Changchun 130026, PR China

ARTICLE INFO

Article history:
Received 1 June 2009
Received in revised form 22 October 2009
Accepted 23 October 2009

Keywords:
Oil shale ash
Azeotropic distillation
Nanoscale
Gamma-alumina

ABSTRACT

A combined process was proposed for the utilization of waste oil shale ash (OSA) in the production of gamma-alumina nanoparticles. The process consisted of two stages, leaching and sintering. The ultrasonic technique followed by a heterogeneous azeotropic distillation process in the presence of polyethylene glycol (PEG) was carried to ensure complete elimination of the residual water in the precipitate. The structural and morphological properties of the calcined nanocrystalline powders were characterized by X-ray diffractometer (XRD), transmission electron microscope (TEM), Brunauer–Emmett–Teller nitrogen-gas adsorption method (BET). The as-prepared precursor hydroxides were analyzed using thermogravimetric–differential thermal analysis (TG–DTA), Fourier transform infrared spectroscopy (FT-IR), and X-ray photoelectron spectroscopy (XPS). The results indicated that the gamma-alumina powder with a uniform particle is well dispersed and the particle size is 20–40 nm; the waste OSA can be utilized to produce gamma-alumina nanoparticles.

1. Introduction

Today, there is a growing interest in developing low-cost energy resource in the world. As a possible alternative, oil shale, which is a natural kerogenous rock, has been used to generate electricity and extract oil for almost a century. A by-product fly ash from oil shale processing is OSA, which is considered as a serious environmental pollutant [1]. Therefore, it is necessary to develop a new approach to OSA management. So far, most research focused on the aspect of building materials [2–7] and adsorbent [8–16]. Synthesizes of tobermorite [17] and calcium-alumino-slicate hydrate [18] have been also reported as possible ways for the utilization of OSA.

Nano-sized alumina has extensive potentiality for being used in chemical absorbent, gas sensor, catalysts, and ceramic raw material. Considerable effort has been put into develop wet chemical synthesis methods because they offer convenient routes for ultrafine and high-purity alumina nanopowder. However, the alumina particles were often found to be agglomerated on drying and calcination. To solve this problem, various methods for the reduction of the particle size have been reported, including sonochemical synthesis [19,20], azeotropic distillation [21,22], and supercritical-water processing [23] and so on.

In this work, we aim to synthesize gamma-alumina nanopowder using OSA as alumina source via the ultrasonic technique in the hydrolysis–condensation stage followed by azeotropic distillation. The dispersion mechanism of gamma-alumina nanopowder is also proposed based on the present experimental facts.

2. Materials and methods

2.1. Raw materials and reagents

Samples of OSA were collected from the factory in Huadian city of Jilin Province. The organic contents (loss-on-ignition, LOI) and metal contents of oil shale are shown in Table 1. The carbon dioxide gas, with a purity of 99.99%, was purchased from Changchun Xinguang Gas Manufacturing Co., Ltd. Other reagents were purchased from Beijing Chemical Reagent Research Institute. All chemical reagents were analytical grade.

2.2. Ultrasonic irradiation facility and parameters

The low powder ultrasonic radiation was performed in an ultrasonic cleaner (KQ-100DB, Kunshan Inc., China) that produced a 40 kHz ultrasound at its bottom. Bath capacity of the sonicator is 3 L. Its power can be changed from 40 to 100 W.

2.3. Experimental procedure

The preparation of the nanoscale alumina from OSA is schematically sketched in the flowchart of Fig. 1 and involves two stages.

* Corresponding author. Tel.: +86 431 88502259.
E-mail address: gansc@jlu.edu.cn (S. Gan).

1385-8947/$ – see front matter © 2009 Elsevier B.V. All rights reserved.
doi:10.1016/j.cej.2009.10.048

Table 1
Chemical component of oil shale and oil shale ash.

Component	% Raw oil shale	% Raw oil shale ash
Silicon dioxide	31.68	63.58
Titanium dioxide	0.39	0.75
Ferric oxide	4.23	5.47
Aluminum oxide	10.77	16.69
Phosphorous pentoxide	0.26	0.26
Manganese oxide	0.05	0.13
Calcium oxide	1.63	5.12
Magnesium oxide	1.84	2.51
Potassium oxide	0.84	1.68
Sodium oxide	0.40	1.02
LOI	47.85	2.24

2.3.1. Leaching of aluminium

A porcelain boat, containing 20 g 120-mesh OSA and 8 g sodium chloride was heated at 700 °C for 3 h and then air-dried. Subsequently, the leaching experiments were performed in a 1000 mL three-necked flask heated in a hemispherical mantle kept constant within ±0.5 °C and connected to a mechanical agitator, equipped with twin-bladed impeller and shaft coated by Teflon. For minimizing aqueous loss, a reflux condenser was applied. After 5 h, the leach liquor was separated from the residue by vacuum filtration. Then, 6 M sodium hydroxide solution was added to the leaching liquor to adjust the pH to 13. After filtration, the supersaturated sodium aluminate solution was obtained, and the aluminum concentration is shown in Table 2.

2.3.2. Synthesis of gamma-alumina nanoparticles

Approximately 0.6 g surfactant (polyethylene glycol, PEG) was added to the supersaturated sodium aluminate solution. To this solution, carbon dioxide was injected until the pH value of the mixture was 9. Under ultrasonic radiation (for 30 min, 60 °C), the reaction mixture was further aged about 11.5 h. The resulting white precipitate was recovered and washed with anhydrous ethanol several times to obtain the as-synthesized product (marked as S_1).

Table 2
Chemical composition of leaching and purified solution of elements.

Element	Leaching solution of OSA ($\mu g\,mL^{-1}$)	Purified solution of OSA ($\mu g\,mL^{-1}$)
Aluminum	985.400	983.900
Calcium	10.170	1.077
Manganese	37.140	7.435
Iron	1.942	0.000
Titanium	0.131	0.000

Subsequently, S_1 was transferred into a rockered flask containing 30 mL of n-butanol. After distilling at 117 °C (the boiling point of n-butanol) for 35 min, the remaining n-butanol was removed through oven-drying (100 °C for 12 h) to obtain loose powder (marked as S_2). This powder was calcined at 550 °C for 2 h to obtain nano-sized gamma-alumina powder.

2.4. Characterization

The chemical compositions of the OSA were determined by X-ray fluorescence (XRF) analysis (PW1404/10. Philips, Holland). The mineral leachates and their purified solution were analyzed using inductively coupled plasma mass spectrometry (ICP-MS), model X Series II, USA. X-ray diffraction (XRD) analysis for powders was carried out by D/Max-IIIC (Rigaku, Japan) with Cu Kα radiation. Powder morphology and dispersity were observed on transmission electron microscope (TEM, JEM-2000EX, Japan). The N_2 adsorption measurement was examined by a surface analyzer (ASAP 2010, USA) and the BET surface area, and the pore volumes were calculated. The pore size distributions were estimated by the Barrette–Joynere–Halenda (BJH) method. Thermogravimetric–differential thermal analysis (TG–DTA) curves of the samples were recorded on a TG-8120 (Rigaku, Japan) using alpha-alumina as the standard materials. Infrared spectra of the samples were investigated on a FT-IR (Nicolet Impact 410, USA) by

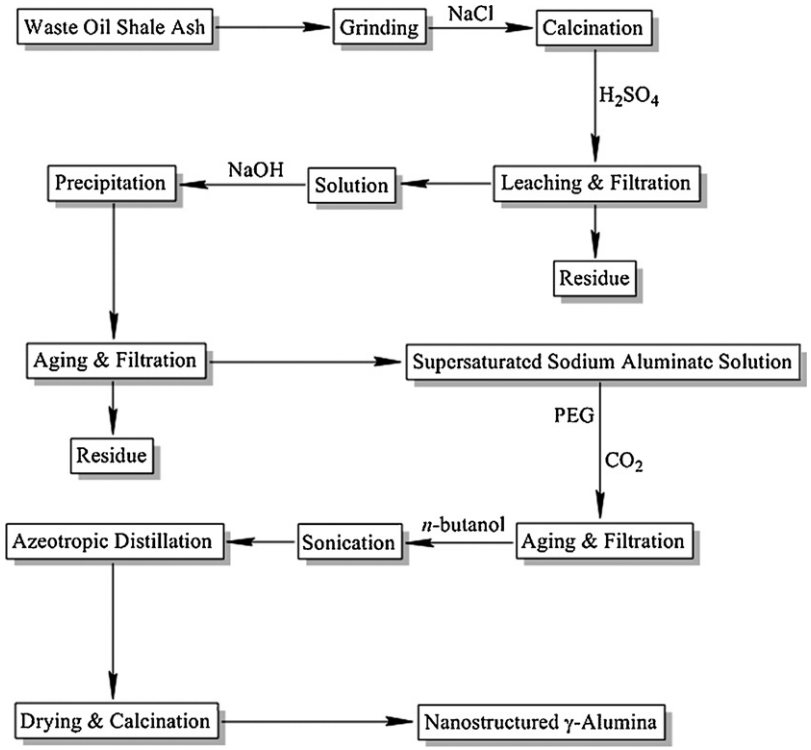

Fig. 1. Flowchart for the synthesis of gamma-alumina nanoparticle.

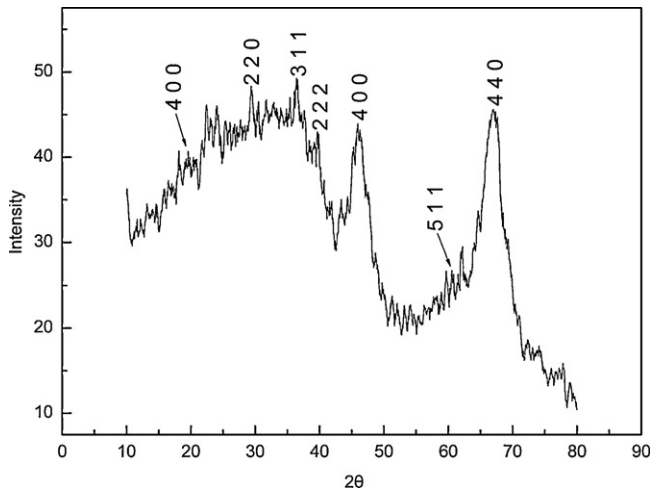

Fig. 2. XRD pattern of the gamma-alumina nanoparticle.

KBr disk method. The surface of precursor was analyzed by X-ray photoelectron spectroscope (XPS) (Thermo ESCALAB 250, UK).

3. Results and discussion

3.1. Characterization

3.1.1. Properties of alumina nanopowder

Representive XRD patterns are shown in Fig. 2 for the as-made gamma-alumina prepared from OSA. The diffraction patterns of the calcined products show consistent with the standard diffraction data for gamma-alumina (JCPDS Card 10-0425). Gamma-alumina, as transition alumina, is disordered crystalline phases formed through the thermal dehydration of aluminum hydroxides and oxy-hydroxides [24]. It can be seen that the widths of the peaks are characteristic of a low-crystalline material as expected for such a low calcinations temperature and short time. On the basis of Scherrer equation, the crystal size of products is calculated from the full width at half-maximum are 16 nm.

Fig. 3 shows the transmission electron microscopy of gamma-alumina. The nanoparticles of the product has good dispersity without hard agglomerate and are uniform in size and shape. The average diameter is 20–40 nm, which is basically in accordance with the XRD results mentioned above. The dispersity of the product is consistent with the TEM result (calcination temperature, 600 °C) reported by Wang et al. [25].

The textural properties of the gamma-alumina powders are further investigated by the N_2 adsorption–desorption and pore size distribution (PSD) analyses. The result shows that the sample has a specific surface area of about 191.7 m^2/g, pore volume of 0.445 cm^3/g, and pore size of 9.2 nm. The nitrogen adsorption–desorption isotherm are shown in Fig. 4. The isotherm obtained for the sample was of type IV which is the characteristic feature of the mesoporous materials [26,27]. The desorption cycles of the isotherm showed a hysteresis loop is attributed to the capillary condensation occurring in the mesopores [28]. The shape of the hysteresis loops is identified with the specific pore shape. The adsorption–desorption branches of the sample is almost parallel and vertical over a wide range of p/p_0 showing the H_1 type of the hysteresis loop. Such type of hysteresis loop is often associated with cylindrical mesopores open at both ends [29].

Fig. 5 depicts that the PSD of the products is trimodal with the peak pore diameters at 3, 16 and 78 nm. This implies that the as-made gamma-alumina consisted of interpenetrating meso- (pores below 50 nm) and macrostructures (pores above 50 nm).

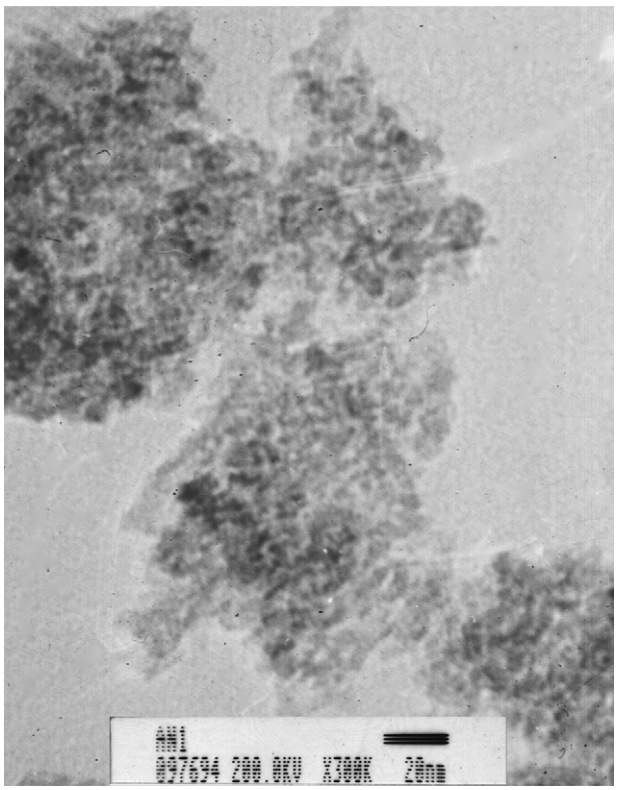

Fig. 3. TEM micrograph of the gamma-alumina nanoparticle.

3.1.2. Properties of precursors

The TG and DTA results for the precursor powder (S_2) are shown in Fig. 6. The TG curve displays two weight-loss stages. The first stage at below 240 °C is associated with the removal of adsorbed water. In this temperature range, the DTA curve show only one endothermic peak at 201 °C, which is attributed to the desorption of the interlayer water. The second stage located at 240–450 °C, the corresponding DTA curve show a broad exothermic peak. Specially, the endothermic peak at 321 °C associated with the phase transformation of transition alumina.

Fig. 7 shows the FT-IR spectra of precursors S_1 and S_2. The main difference between S_1 and S_2 is the adsorption bands at 2915 and 2847 cm^{-1}, which can be attributed to the vibration of $-CH_2-$ groups of butanol and PEG [30]. And the peak at 1377 cm^{-1} (S_2) is

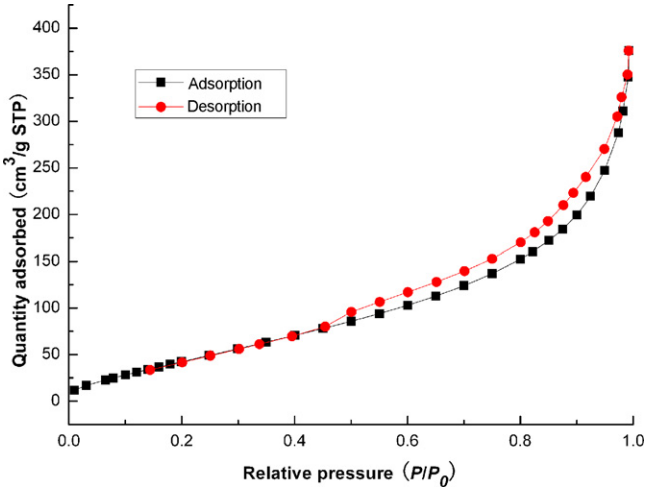

Fig. 4. N_2 adsorption–desorption isotherm of the gamma-alumina nanoparticle.

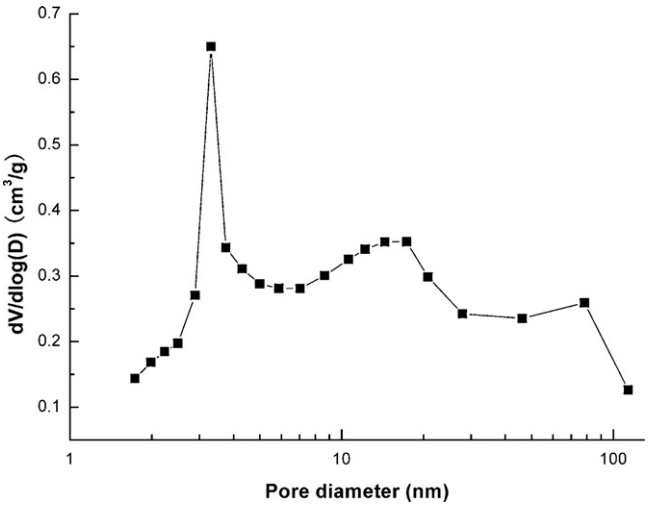

Fig. 5. Pore size distribution of the gamma-alumina nanoparticle.

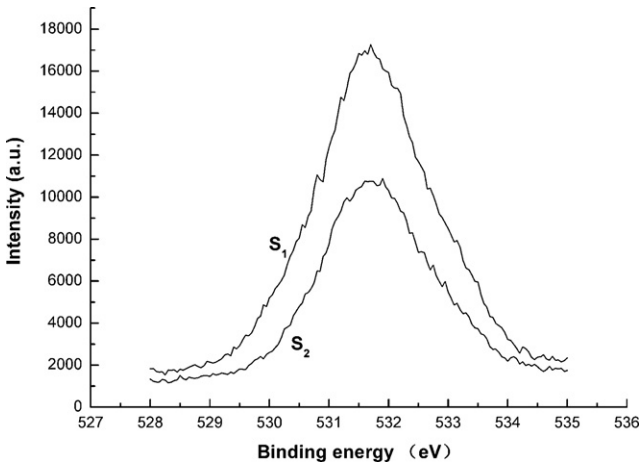

Fig. 8. XPS spectra of S_x series of precursors.

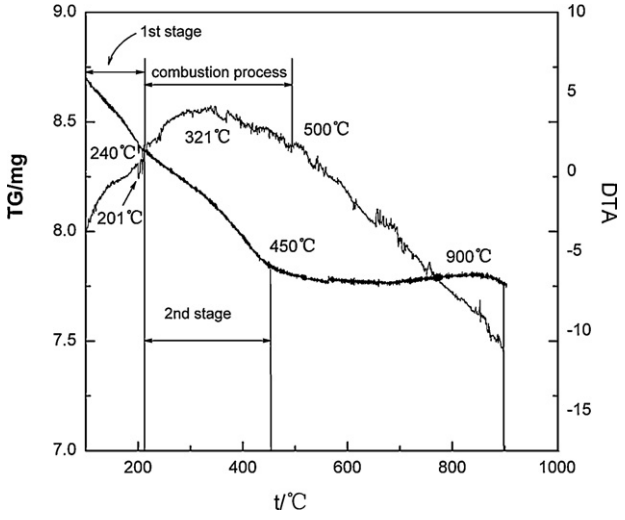

Fig. 6. TG–DTA curves of precursors.

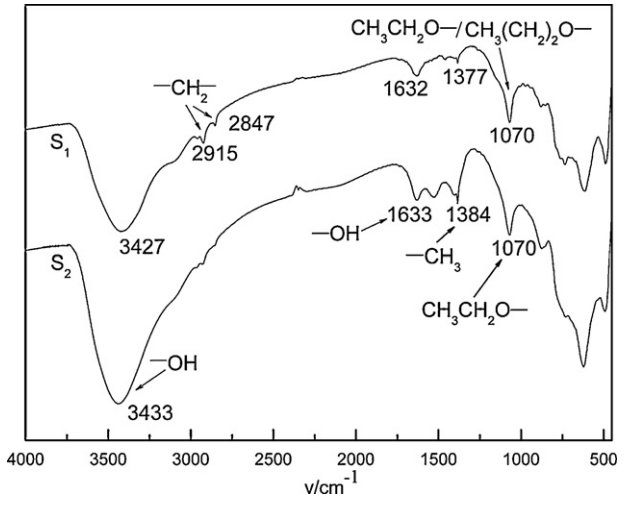

Fig. 7. FT-IR spectra of S_x series of precursors.

coherent with δ_3 vibration of CH_3– groups, implying the presence of n-butanol. The adsorption peak at 1633 cm^{-1} (S_1) and 1632 cm^{-1} (S_2) are attributed to the complex peak of the excess water intercalated in the layers of precursors [31] and –OH groups on the surface of aluminium hydroxide and alcohol [32]. The C–O stretching vibration peak of CH_3CH_2O– or $CH_3(CH_2)_2O$– groups at 1070 cm^{-1} (S_1, S_2) can also be monitored. The adsorption at 3433 and 3427 cm^{-1} (S_1, S_2) are associated to the hydroxyls on the precursor surface.

Fig. 8 is the XPS spectra of pristine precursor (S_1) and butanol-coated precursor (S_2). For S_1, the O 1s core level spectrum presents peak at binding energy of 531.79 ± 0.10 eV, which associates with –OH groups in AlOOH structure. After coating, O 1s peak appears at lower energy of 531.59 ± 0.10 eV and its intensity decreases significantly. This is because the presence of O 1s peak from the Al–O–C_4H_9 groups. This suggests that some n-butanol molecules are chemisorbed on the surface of the precursors. The result also agrees with the FT-IR analysis.

3.2. Overview of the synthesis process

The chemical compositions of the OSA before and after the leaching process are presented in Table 2. It can be seen, the thermal and acid treatments are efficient, resulting in a high-purity aluminum solution with very low level of remaining calcium and magnesium.

During the present precipitation process, the distribution of alumina nanopowder indicates the particle size of precursor is quite small. Also, the precursor has good chemical reactivity due to the crystal defects result from the ultrasound radiation [33]. Therefore, the obtained crystal of aluminum hydroxide is important for nanoceramics and could even be used as seed particles in the Bayer process. Additionally, it should be note that ultrasound can accelerate the breeding nucleation [34].

3.3. Powder dispersion

Hard agglomeration occurs upon drying and calcinations due to the hydrogen bonds between water molecules and surface –OH groups on particles. In the present investigation, we combine the azeotropic distillation with surface modification and sonication to prevent hard agglomeration. The experiments show that the products as-made are well dispersed, and the possible dispersion mechanism of this combined method can be depicted as follows.

PEG is terminated by alcohol groups that render it reactive with respect to the surface hydroxyls of the powder [35]:

$$\equiv Al\text{–}OH + HO(CH_2CH_2O)R \rightarrow \equiv Al\text{–}O\text{–}(CH_2CH_2O)_xR + H_2O$$

During the present precipitation process, PEG adsorbed on the surface of the formed aluminum hydrate. Therefore, the accessibility is decreased due to the spatial effects of PEG molecular. On the other hand, the porous structures of the nanoparticles could be attributed to the combustion of the coated PEG and n-butanol during the calcination.

Ultrasonic radiation is an effective method to prepare nanoscale ultrafine powder [36–38]. It is known that 20 kHz ultrasonic radiation can rupture chemical bonds effectively [39] and so large aggregates are not obtained using this technique. Also, the other two aspects should be noted: (1) during the present precipitation process, PEG can adsorb on the surface of the formed aluminum hydrate. The coated PEG would prevent the hydrogen bonding formed between the neighbouring particles. On the other hand, a quick coagulation of the formed colloids would lead to the formation of loose particles with large particle size, and meantime, large amount of PEG would be enfolded in these loose particles, which would weaken dispersion effect of PEG. Herein, the sonication can destroy the loose particles and then result in the re-adsorption of PEG on the formed particles. (2) n-Butanol was selected in this work because of its highest water content in the azeotrope (44.5 wt%) among several practicable water–organic binary systems [40]. However, only about 10 wt% of water is miscible in n-butanol at room temperature. Sonication enhanced the mixing of the hydrous gel and n-butanol, which would benefit the dehydration of the following azeotropic distillation process.

Azeotropic distillation can remove the terminal hydroxyl groups and physically adsorbed water molecules on particle surface via distillation by forming water–organic solvent binary azeotrope. The butoxy could replace the H_2O/OH groups of the precipitate with a hydrophobic tail outside. The IR bands in Fig. 7 can certify the presence of n-butanol in the precipitate. Large quantity of adsorbed water is squeezed out due to the compact stacking of organic species on the surface of inorganic precursors [41]. This result is confirmed by the TG–DTA analysis.

4. Conclusions

Nanostructured gamma-alumina powder has been prepared from OSA. Azeotropic distillation combine with ultrasound irradiation and surfactant modification effectively dehydrate hydrous alumina gel and thus prevent the formation of hard agglomerations. Calcinations product of the gamma-alumina particles exhibited uniform shapes. The approach presented herein might be applied to the production of gamma-alumina nanoscale powder. Furthermore, it opens a new way of promising application of OSA.

Acknowledgements

This work has been funded by the Scientific Research Program No.: 20051015, Development Program of China (863 Program, Grant 2007AA06Z202) and No.: 20070405.

References

[1] R. Shawabkeh, A. Al-Harahsheh, M. Hami, A. Khlaifat, Conversion of oil shale ash into zeolite for cadmium and lead removal from wastewater, Fuel 83 (2004) 981–985.
[2] M.M. Smadi, R.H. Haddad, The use of oil shale ash in Portland cement concrete, Cement Concrete Comp. 25 (2003) 43–50.
[3] V.A. Mymrin, H.A. Ponte, Oil-shale fly ash utilization as independent binder of natural clayey soils for road and airfield base construction, Particul. Sci. Technol. 23 (2005) 99–107.
[4] I. Asi, A. Assa'ad, Effect of Jordanian oil shale fly ash on asphalt mixes, J. Mater. Civil Eng. 17 (2005) 553–559.
[5] Y. Awni. Al-Otoom, Utilization of oil shale in the production of Portland clinker, Cement Concrete Comp. 28 (2006) 3–11.
[6] X.M. Jiang, X.X. Han, Z.G. Cui, New technology for the comprehensive utilization of Chinese oil shale resources, Energy 32 (2007) 772–777.
[7] O.A. Ehinola, Q.S. Zhu, Utilization of Lokpanta oil shale in Portland cement manufacturing in Nigeria: a thermodynamic approach, Oil Shale 25 (2008) 310–327.
[8] Z. Al-Qodah, Adsorption of dyes using shale oil ash, Water Res. 34 (2000) 4295–4303.
[9] Z. Al-Qodah, W. Lafi, Adsorption of reactive dyes using shale oil shale ash in fixed beds, J. Water Supply Res. T. 52 (2003) 189–198.
[10] R.A. Shawabkeh, A. Al-Harahsheh, M. Hami, A. Khlaifat, Conversion of oil shale ash into zeolite for cadmium and lead removal from wastewater, Fuel 83 (2004) 981–985.
[11] R. Shawabkeh, A. Al-Harahsheh, A. Al-Otoom, Production of zeolite from Jordanian oil shale ash and application for zinc removal from wastewater, Oil Shale 21 (2004) 125–136.
[12] R. Shawabkeh, A. Al-Harahsheh, A. Al-Otoom, Copper zinc sorption by treated oil shale ash, Sep. Purif. Technol. 40 (2004) 251–257.
[13] N.R.C.F. Machado, D.M.M. Miotto, Synthesis of Na–A and –X zeolites from oil shale ash, Fuel 84 (2005) 2289–2294.
[14] Z. Al-Qodaha, A.T. Shawaqfehb, W.K. Lafia, Adsorption of pesticides from aqueous solutions using oil shale ash, Desalination 208 (2007) 294–301.
[15] R. Shawabkeh, A. Harahsheh, H_2S removal from sour liquefied petroleum gas using Jordanian oil shale ash, Oil Shale 24 (2007) 109–116.
[16] A. Kaasik, C. Vohla, R. Motlep, U. Mander, K. Kirsimae, Hydrated calcareous oil-shale ash as potential filter media for phosphorus removal in constructed wetlands, Water Res. 42 (2008) 1315–1323.
[17] J. Reinik, I. Heinmaa, J.P. Mikkola, U. Kirso, Hydrothermal alkaline treatment of oil shale ash for synthesis of tobermorites, Fuel 86 (2007) 669–676.
[18] J. Reinik, I. Heinmaa, J.P. Mikkola, U. Kirso, Synthesis and characterization of calcium-alumino-silicate hydrate from oil shale ash—towards industrial applications, Fuel 87 (2008) 1998–2003.
[19] S. Ramesh, E. Sominska, B. Cina, R. Chaim, A. Gedanken, Nanocrystalline γ-alumina synthesized by sonohydrolysis of alkoxide precursor in the presence of organic acids: structure and morphological properties, J. Am. Ceram. Soc. 83 (2000) 89–94.
[20] T. Chave, S.I. Nikitenko, D. Granier, T. Zemb, Sonochemical reactions with mesoporous alumina, Ultrason. Sonochem. 16 (2009) 481–487.
[21] X. Liu, Z. Wu, T. Peng, P. Cai, H. Lv, W. Lian, Fabrication of alumina nanofibers by precipitation reaction combined with heterogeneous azeotropic distillation process, Mater. Res. Bull. 44 (2009) 160–167.
[22] R.Y. Hong, T.T. Pan, J.Z. Qian, H.Z. Li, Synthesis and surface modification of ZnO nanoparticles, Chem. Eng. J. 119 (2006) 71–81.
[23] R. Viswanathan, G.D. Lilly, W.F. Gale, R.B. Gupta, Formation of zinc oxide–titanium dioxide composite nanoparticles in supercritical water, Ind. Eng. Chem. Res. 42 (2003) 5535–5540.
[24] K. Wefers, C. Misra, Oxides and hydroxides of aluminum, Alcoa Technical Paper No. 19, Revised, Alcoa Laboratories: Alcoa Center, PA, 1987 (quoted in Z.R. Zhang, R.W. Hicks, T.R. Pauly, T.J. Pinnavaia, Mesostructured Forms of γ-Al_2O_3, J. Am. Chem. Soc. 124 (2002) 1592–1593).
[25] S.Y. Wang, X.A. Li, S.F. Wang, Y. Li, Y.C. Zhai, Synthesis of γ-alumina via precipitation in ethanol, Mater. Lett. 62 (2008) 3552–3554.
[26] W.C. Li, A.H. Lu, S.C. Guo, Control of mesoporous structure of aerogels derived from cresol-formaldehyde, J. Colloid Interf. Sci. 254 (2002) 153–157.
[27] A.C. Pierre, E. Elaloui, G.M. Pajonk, Comparison of the structure and porous texture of alumina gels synthesized by different methods, Langmuir 14 (1998) 66–73.
[28] A. Parvathy Rao, A. Venkateswara Rao, G.M. Pajonk, Hydrophobic and physical properties of the ambient pressure dried silica aerogels with sodium silicate precursor using various surface modification agents, Appl. Surf. Sci. 253 (2007) 6032–6040.
[29] J.L. Mohanan, S.L. Brock, Influence of synthetic and processing parameters on the surface area, speciation, and particle formation in copper oxide/silica aerogel composites, Langmuir 15 (2003) 2567–2576.
[30] L.J. Michot, O. Barres, E.L. Hegg, T.J. Pinnavaia, Cointercalation of aluminum (A13) polycations and nonionic surfactants in montmorillonite clay, Langmuir 9 (1993) 1794–1800.
[31] L. Ji, J. Lin, K.L. Tan, H.C. Zeng, Synthesis of high-surface-area alumina using aluminum tri-secbutoxide-2,4-pentanedione-2-propanol-nitric acid precursors, Chem. Mater. 12 (2000) 931–939.
[32] S. Cabrera, J.E. Haskouri, J. Alamo, A. Beltran, D. Beltran, S. Mendioroz, M.D. Marcos, P. Amoros, Surfactant-assisted synthesis is of mesoporous alumina showing continuously adjustable pore sizes, Adv. Mater. 11 (1999) 379–381.
[33] H. Li, H. Li, Z.C. Guo, Y. Liu, The application of power ultrasound to reaction crystallization, Ultrason. Sonochem. 13 (2006) 359–363.
[34] B. Zhang, J. Li, Q.Y. Chen, G.H. Chen, Precipitation of $Al(OH)_3$ crystals from supersaturated sodium aluminate solution irradiated with ultrasonic sound, Miner. Eng. 22 (2009) 853–858.
[35] M.L. Green, W.E. Rhine, P. Calvert, H.K. Bowen, Preparation of poly(ethylene glycol)-grafted alumina, J. Mater. Sci. Lett. 12 (1993) 1425–1427.
[36] B. Neppolian, Q. Wang, H. Jung, H. Choi, Ultrasonic-assisted sol–gel method of preparation of TiO_2 nano-particles: characterization, properties and 4-chlorophenol removal application, Ultrason. Sonochem. 15 (2008) 649–658.

[37] J.H. Bang, K.S. Suslick, Sonochemical synthesis of nanosized hollow hematite, J. Am. Chem. Soc. 129 (2007) 2242–2243.
[38] S.F. Wang, F. Gu, M.K. Lu, Sonochemical synthesis of hollow PbS nanospheres, Langmuir 22 (2006) 398–401.
[39] A. Gedanken, Using sonochemistry for the fabrication of nanomaterials, Ultrason. Sonochem. 11 (2004) 47–55.
[40] H.B. Qiu, L. Gao, C.D. Feng, J.K. Guo, D.S. Yan, Preparation and characterization of nanoscale Y-TZP powder by heterogeneous azeotropic distillation, J. Mater. Sci. 30 (1995) 5508–5513.
[41] H.Y. Zhu, J.D. Riches, J.C. Barry, γ-Alumina nanofibers prepared from aluminum hydrate with poly(ethylene oxide) surfactant, Chem. Mater. 14 (2002) 2086–2093.